J. Fluid Mech. (1981), *vol.* 103, *pp.* 33–51
Printed in Great Britain

The phase-averaged large-scale structures in three-dimensional turbulent wakes

By A. E. PERRY AND J. H. WATMUFF
Department of Mechanical Engineering, University of Melbourne, Parkville, 3052

(Received 30 May 1979 and in revised form 7 April 1980)

Experiments are described which show that large-scale coherent structures exist in the wakes behind three-dimensional blunt bodies. Using a 'flying hot-wire' apparatus, the vortex-shedding cycle has been described by phase-averaged vector fields allowing an animation of large-scale motions to be produced. It is found that the large-scale structures retain their identity for long streamwise distances and contribute significantly to the Reynolds stress.

Using critical-point theory as described recently by Perry, Lim & Chong (1980), the effect of phase 'jitter' on 'washout' has been analysed. Furthermore, it is found from critical-point theory that the large-scale motions possess the same geometrical features as the low-Reynolds number (unsteady laminar flow) wake results of Perry & Lim (1978) and Perry *et al.* (1980).

1. Introduction

The aim of this work is to see whether any statistical measurements based on phase of vortex shedding could be made which would reveal the shape of representative large-scale eddy structures behind blunt three-dimensional bodies at high Reynolds numbers. Conventional statistical measurements fail to give this insight. The authors find that, even with the crudest forms of phase detection, recognizable structures and patterns emerge. Not only can they be recognized and seen to retain their identity for long streamwise distances, but the large-scale entrainment processes are also evident and are consistent with the low-Reynolds-number non-turbulent results of Perry *et al.* (1980).

Perry & Lim (1978) performed a series of experimental investigations of coflowing wakes and jets at Reynolds numbers of the order 300 to 1000. Smoke was observed issuing from a glass tube and structures were seen to form in the smoke and they remained coherent for long streamwise distances. They defined coherence to mean that eddying motions retain their identity even though their shape, velocity and length scales undergo continual change as they are convected downstream. The structures were seen to modulate in scale and frequency and, in order to study them in detail, the tube was subjected to a small lateral oscillation. The structures were then 'locked in' and they appeared perfectly frozen when viewed under stroboscopic light. The velocity at a given point therefore was perfectly periodic in time.

The existence of coherent large-scale structures behind bodies at high Reynolds numbers is well established (e.g. see the flow-visualization studies by Papailiou & Lykoudis (1974) for the wake behind a cylinder). Perry & Lim conjectured that their

0022–1120/81/4604–2880 $02.00

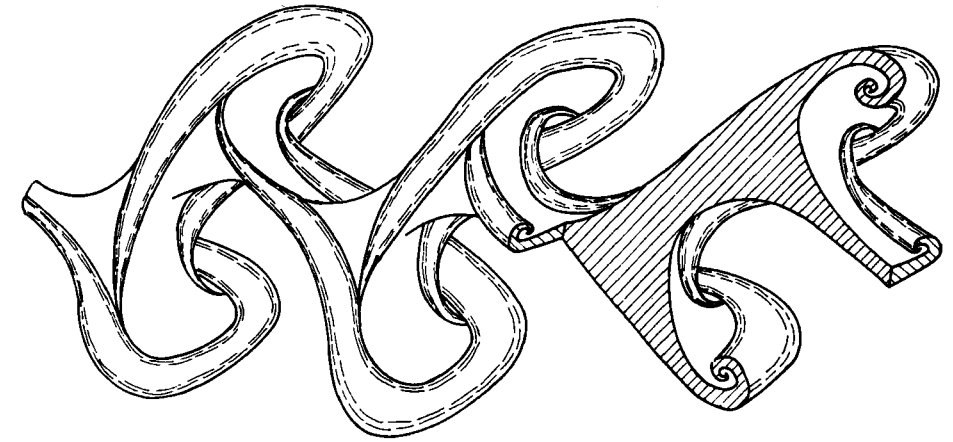

(a)

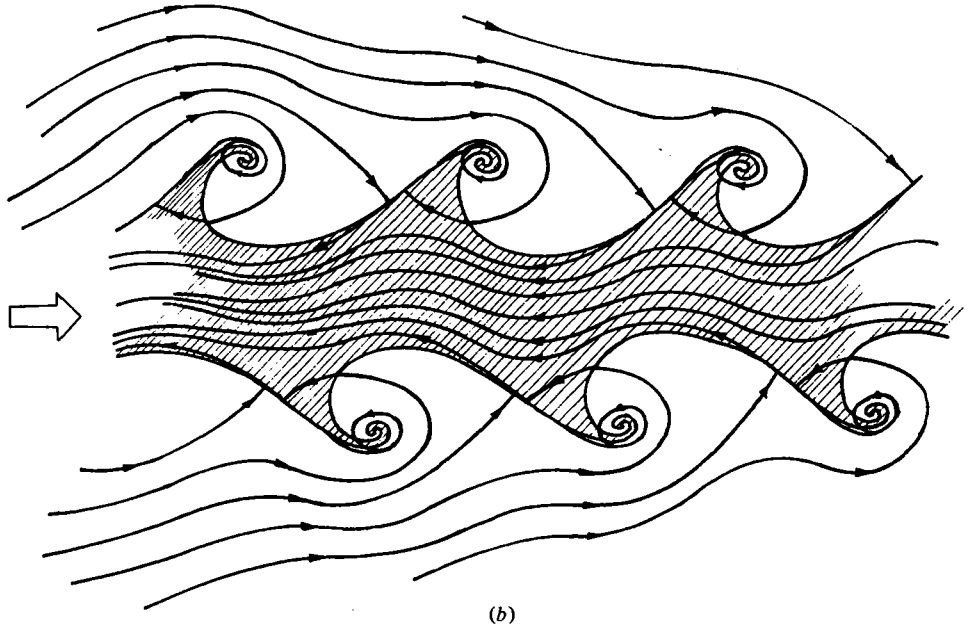

(b)

FIGURE 1. Interpretations of three-dimensional wake structures. (a) Interpretation of the way the smoke (i.e. the cylindrical vortex sheet) is folded in a coflowing wake (after Perry *et al.* 1980). (b) Interpretation of the instantaneous streamline pattern as seen by an observer moving with the structures given in (a) above. Cross-hatching indicates the smoke (after Perry *et al.* 1980). In wakes behind bodies, cross-hatching would indicate boundary-layer material and hatched zones would be much narrower.

'frozen' structures might have relevance to these large-scale structures of turbulence. There is some evidence for this. For example, the low-Reynolds-number positively buoyant jets (e.g. cigarette smoke) bear a strong resemblance to the high-Reynolds-number flow of smoke issuing from a chimney in cross-flow (see figure 6 of Perry & Lim).

Of particular interest to the work reported here are the neutrally buoyant co-

flowing wakes shown issuing from a tube illustrated in their figure 5(*b*). It was found that these structures bear a strong resemblance to the naturally occurring (i.e. no forcing) wake behind a three-dimensional blunt body as shown in their figure 5(*f*). These structures are the three-dimensional version of the classical von Kármán vortex street. In the case of coflowing wakes a cavity need not occur but, in the case of blunt bodies, the volume flow of boundary-layer material which comprises the coflowing component is usually so small that a cavity does occur. However, the flow beyond the cavity of a body does indeed resemble the coflowing wakes of Perry & Lim.

Recently, Perry *et al.* (1980) performed hot-wire measurements of these types of structures using a phase-averaging technique and velocity fields were interpreted with the aid of critical-point theory. Figures 1(*a*) and (*b*) show their interpretations and the deduced instantaneous streamline pattern as seen by an observer moving with the structures. The authors set out to produce a corresponding vector field plot for the high-Reynolds-number case and to utilize the critical-point theory given in Perry *et al.* for interpreting the patterns which emerge.

Because the structures of Perry *et al.* (1980) were so periodic in time, the vector fields could be produced by conditionally sampling data on the basis of the precise phase of tube oscillation. The periodicity of the velocity field meant that only 10 samples at each point and phase were needed for convergence of the phase-averaged data. However in the high-Reynolds-number flow the large-scale motions modulate in frequency and scale (phase jitter) and superimposed on these large motions are fine-scale motions containing appreciable turbulent energy. Far more data are needed before convergence is achieved so that the fine-scale motions and 'phase jitter' are averaged out.

Cantwell (1975) studied the near wake of a two-dimensional circular cylinder at a Reynolds number of 140000. A sensor responding to surface pressure variations was used to detect the phase of the vortex shedding as signals from crossed-wire probes attached to whirling arms were sampled at closely spaced points in the near wake. The whirling arms were used to subject the wires to an additional bias velocity to remove the flow directional ambiguity problems in the cavity of the cylinder where reverse flow was occurring. By sorting the data taken at each point into 16 groups corresponding to successive phase intervals of the surface pressure signal, the fine-scale motions were averaged out, resulting in a 16-frame animation of the entire measured field in terms of the large-scale motions. The phase-averaging technique revealed coherent structures having an appearance resembling the computed results of the classical von Kármán potential flow solution, which is known to be applicable at Reynolds numbers of order 1000. Cantwell pioneered the technique of rapidly sampling data from wires moving through a flow. The authors have extended the technique in the present work and have modified it to produce results more rapidly and with far less data storage problems than experienced by Cantwell.

2. Apparatus and procedure

Figure 2 shows a schematic layout of the apparatus used by the authors. A crossed-wire probe was attached to a sting fastened to an air-bearing sled which rode on the top of the wind tunnel working section. The sting passed through a slot cut in the working-section roof and the sled was propelled back and forth continually by means

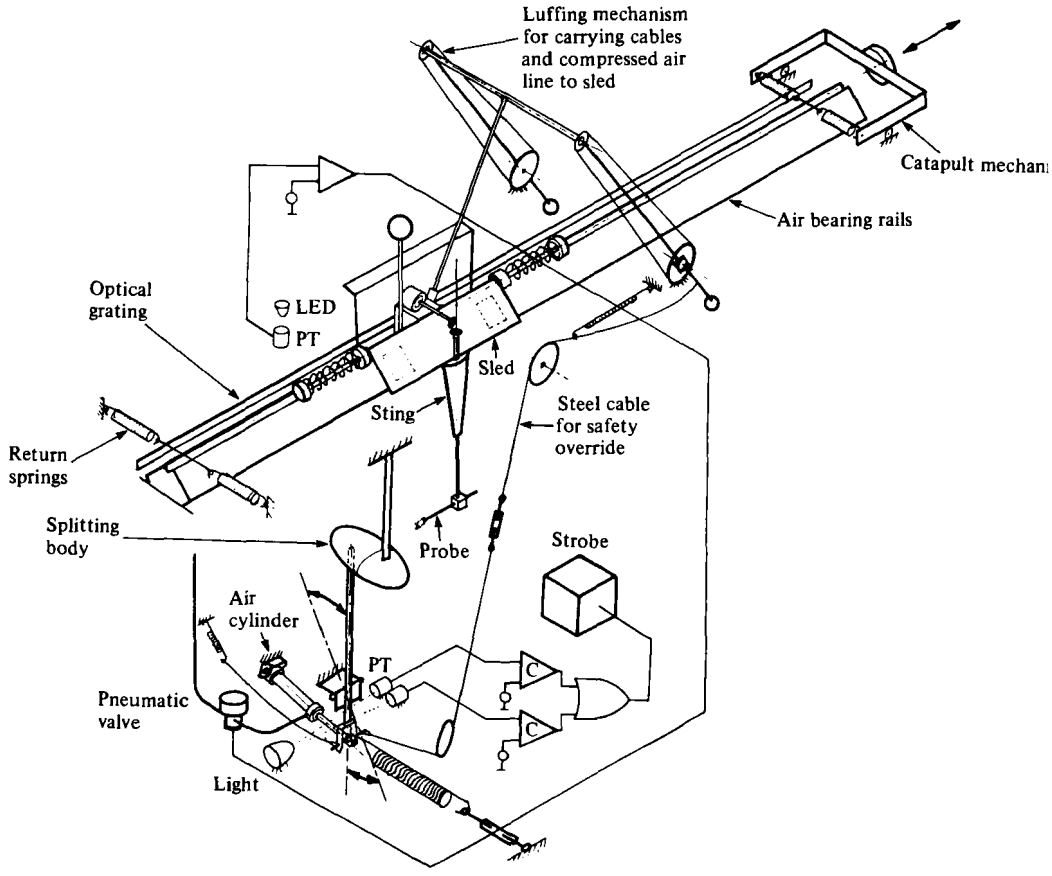

FIGURE 2. Overall layout of flying hot-wire machinery. Mechanism for splitting the body to enable wires to pass through cavity and body also shown. PT means photo-transistor. C means comparator. Strobe was used for indicating position of probe on opening of body. The photo-transistors for computer control and data acquisition are not shown.

of a catapult mechanism at the downstream end and a return spring system at the other end. The luffing mechanism shown carried a compressed air line to the sled and electrical cables to the probe and the stepping motor vertical-traversing drive. The flow in the near and far wakes of a three-dimensional blunt body was sampled as the sled was moving upstream towards the body. As in Cantwell's experiment the superimposed bias velocity of the wires meant that measurements could be taken in regions of reversed flow without the problems of directional ambiguity. The flow was rapidly sampled at closely spaced points along horizontal rows of the working section using a computer-controlled data acquisition system. This system consisted of an EAI TR48 analog computer and logic box in line before a PDP 11–10 digital computer fitted with a Laboratory Peripheral System (LPS).

The position of the wires along the tunnel was monitored very accurately by counting pulses from a photo-detector system attached to the sled. The photo-detector system rode past a grating producing a pulse every millimetre of sled movement. These pulses were used to control the sampling of data. The velocity of the sled was obtained by demodulating the frequency of the pulses in much the same way as does an analog

LDV processor. During the sled motion, the phase of the vortex-shedding process behind the blunt body and the sled velocity were also recorded. At the end of a sled pass, the data taken at each point along a row were sorted into one of sixteen groups, each corresponding to an interval of the phase of the vortex-shedding cycle. The bias velocity of the sled improved the linearity of the hot wires, and the authors found that the variance of the data for a fixed position and phase were sufficiently small to assume linearity and hence voltages could be averaged first before converting the data to phase-averaged velocities. By repeating the process along different rows, sixteen phase-averaged vector plots of the measured flow field were obtained. Cantwell did not assume this linearity, which meant that he had to store each individual sampled voltage for post-experimental processing, using a nonlinear hot-wire calibration inversion program.

The analog computer was used to scale the two hot-wire channel voltages and combine them in such a way as to produce a voltage E_1 sensitive only to streamwise velocity perturbations (u') and a voltage E_2 sensitive only to vertical velo ity perturbations (v') over the range of operating points to be experienced by the wires. This 'matching' procedure could be carried out very accurately and rapidly using two shakers. The dynamic calibrator of Perry & Morrison (1971) was modified to shake the sled back and forth sinusoidally to provide the u' perturbation. Another dynamic calibrator was used to impose vertical sinusoidal velocity perturbations (v') *in situ*. Once the matching procedure was completed the wires and circuits were then dynamically calibrated using the techniques of Perry & Morrison. These techniques were improved by using digital methods. The operating point of the wires was defined by the voltages E_1 and E_2, which are nonlinear functions of velocity. A second-order polynomial curve fit was applied to these nonlinear functions over the range of operating points used in the experiments.

The first- and second-order coefficients of this polynomial were obtained from the dynamic calibrations and the zeroth-order term was obtained from a static calibration. Agreement of the polynomial to the static data points was excellent over the operating range used. The analog computer was also used to subtract bias voltages at various points in the circuits so that the voltage perturbations could be amplified to fill the voltage window of the computer and thus provide maximum numerical resolution. The hot-wire calibrations required no assumptions regarding wire angles nor was any form of heat-transfer law needed.

The greatest problem with the calibrations came from drift with time. Eddying motions are best viewed in a frame of reference moving with their convection velocity. In practice this is achieved by subtracting the mean convection velocity from the results before they are plotted. Hence, the geometry of the eddying motions critically depend on the phase-averaged perturbations. Drift in the hot-wire calibrations was of order of 2% of the inferred mean velocity over the typically 15 h required for an experiment. This small drift had a measurable effect on the patterns and showed up as discontinuities in the vector field between rows. Its effect on a given row was to uniformly influence the temporal mean velocities. The effects on the phase-averaged perturbations were of second order and negligible. The resulting discontinuity from row to row in the vector field was corrected by using information obtained from the traversing of the flow at two fixed streamwise locations with the same crossed-wire probe at the end of the experiments.

One method of detecting vortex shedding was to use a stationary hot wire located in the wake. The pseudo-periodic signal was bandpass filtered to remove high-frequency components and the resulting signal was passed through a comparator. Each leading edge of the comparator output was defined to be the beginning of a new cycle and the time interval between the leading edges was divided up into 16 phase intervals by the computer software. Since the data were sorted into phase boxes $\frac{1}{16}$ of a cycle wide, attempts to obtain spatial resolution better than $\frac{1}{16}$ of a structure wavelength is pointless. This meant that high-frequency components of the signals from the moving probe could be removed by low-pass filtering them at a frequency of an order of magnitude greater than the frequency of vortex shedding. The authors found by experiment that filtering the hot-wire signals increased the rate of data convergence by an order of magnitude. A further means of reducing running time was to use multiple-point smoothing along each row of data of constant phase. The smoothing process consisted of averaging data at a given point with neighbouring points, taking into account the number of samples at each point.

A special program was used to display successive phase-averaged voltages on an oscilloscope. To the eye the animation appeared to be like a wave form propagating across the screen. By collecting data along just one row with uncalibrated wires, one could know after 45 min running time whether phase-averaged coherent structures were present without having to measure the entire flow field.

It is anticipated that a complete detailed report on the apparatus, methods of hot-wire calibration and data reduction will be published. Such information is at present contained in a thesis by Watmuff (1979).

3. Critical-point theory and the effect of phase jitter

At the outset it will be assumed that the inviscid constant vorticity critical-point theory applied by Perry *et al.* to unsteady laminar flow patterns can also be applied to each instantaneous large-scale structure, i.e. the effect of fine-scale motions are being ignored. Perry & Fairlie (1974, 1975) applied this critical-point theory to a stationary turbulent separation bubble with some success. Three types of critical points are needed for the work described here. These are two regular critical points, namely the centre and the saddle, and one irregular critical point, namely the 'dislocated' saddle sitting on a vortex sheet. These critical points are the salient features of eddying motions and it will be assumed that they are translating with a uniform velocity with the structures. When viewed in this frame of reference the centres correspond with pressure minima and saddles with pressure maxima.

Figure 3 shows a conjectured wake behind a blunt body at two instants of time. Here, the vortex-shedding process is not perfectly periodic and the eddy structures modulate in frequency and scale. Also shown in the figure are wave forms from a phase detector where the leading edge of the phase detector signal is arbitrarily shown to represent the beginning of a vortex-shedding cycle. At the two instants shown, the phase detector indicates that the patterns are at the same phase. However it can be seen that eddy A and eddy A' downstream of the phase detector are in quite different locations. Hence eddies which are being phase averaged in this vicinity will be randomly positioned according to some probability density function (p.d.f.) as illustrated in the figure. This random positioning of the eddies at a given phase will be referred

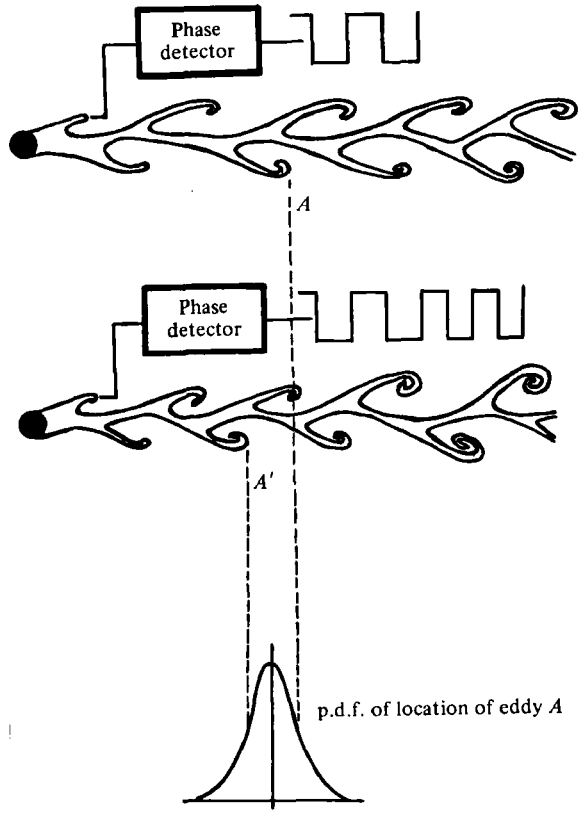

FIGURE 3. Phase jitter. Frequency modulation causes downstream eddies to appear in different locations although the phase detector indicates the same phase.

to here as 'phase jitter' and, if it is large enough, 'washout' of the phase-averaged data will occur. The further downstream one goes, the larger will be the phase jitter and the broader will be the spread of the p.d.f. and hence the larger will be the washout.

The main source of the jitter is of course in the randomness of the vortex shedding but this may be enhanced by other effects, such as phase changes through analog filters, amplitude modulation of signals going to comparators and the arbitrary way phase is assigned by the computer software.

To investigate the effects of jitter one could consider simple flow patterns with critical points, randomize their positions and look at the properties of the averaged patterns. Close to a regular critical point the velocity components vary linearly with distance from the critical point and to this linearized approximation the vorticity is constant. Along any particular ray emanating from the critical point

$$|\mathbf{u}| = Kr, \tag{1}$$

where $\mathbf{u}$ is the velocity vector and r is the distance along the ray. The constant K will be referred to as the 'strength' of the pattern. Let the velocity distribution given by (1) be perturbed by shifting bodily the critical point in a random fashion described by an arbitrary p.d.f. Then the ensemble average of the velocity distribution will remain

unaltered from that given by (1) provided that the mean of the p.d.f. is at $r = 0$. Thus the average of a 'jittered' regular critical point is the same as the unjittered case.

Now, consider the pressure distribution about a jittered critical point. The pressure distribution about an unjittered critical point possesses circular isobars which belong to a parabola of revolution (Perry & Fairlie (1974), Perry *et al.* (1980)) with the axis of symmetry passing through the critical point. Since the slope of the pressure distribution is linear with r for the unjittered critical point, so also will be the slope of the pressure distribution of the averaged critical point. Hence the second derivative or curvature of the pressure distribution after averaging remains unaltered, but the pressure maximum or minimum is altered. The second derivative of pressure, together with the vorticity, controls the pattern. Hence the averaged regular critical point when expressed in terms of mean flow quantities follows the same laws as for the unjittered critical point as expressed by Perry & Fairlie and Perry *et al.* If the scale of jittering of a regular critical point exceeds the scale of the region of linearity, then the averaged flow will still exhibit the critical point but its strength will be diminished and it will be distorted. If the degree of jitter is greater than or equal to a wavelength of a coherent structure then complete washout may occur.

Phase-plane portraits of nonlinear dynamical systems are very useful for generating patterns which possess similar geometrical properties to eddying motions. The phase plane of a simple pendulum is described by the nonlinear differential equation,

$$\ddot{\theta}+\frac{g}{l}\sin\theta = 0, \tag{2}$$

where θ is the amplitude of oscillation, g is the acceleration due to gravity and l is the pendulum length. This system is conservative so that only centres and saddles appear in the phase plane. By putting

$$x_1 = \theta, \quad x_2 = \dot{\theta}, \tag{3), (4}$$

the instantaneous velocity of any solution point as it moves along its solution trajectory is given by

$$u = \dot{x}_1 = x_2, \tag{5}$$

$$v = \dot{x}_2 = -(g/l)\sin x_1. \tag{6}$$

The velocities at a grid of points can be represented by velocity vectors as illustrated in figure 4(*a*). The pattern of velocity vectors shows a resemblance to flows in which only two-dimensional critical points (centres and saddles) appear. For example, the phase plane bears a resemblance to the flow pattern in a two-dimensional shear layer as seen by an observer moving with the structures, i.e. the Kelvin–Helmholtz-like roll-up of a vortex sheet possesses these 'cat's eye' patterns. In fact equations (5) and (6) satisfy the continuity equation and are asymptotic solutions of the Navier–Stokes equations close to the critical points. Far from the critical points the solutions are nonlinear and depart from the Navier–Stokes equations. Nevertheless this phase plane will serve as a useful mathematical model to illustrate certain effects which occur when real flows are phase averaged.

Randomization or jittering of the pendulum phase plane can be accomplished as follows. Imagine that the 'pendulum eddies' are convecting past a stationary reference such that the convection velocity (defined by the product of frequency and structure wavelength) is constant. When a phase-plane centre passes the stationary reference

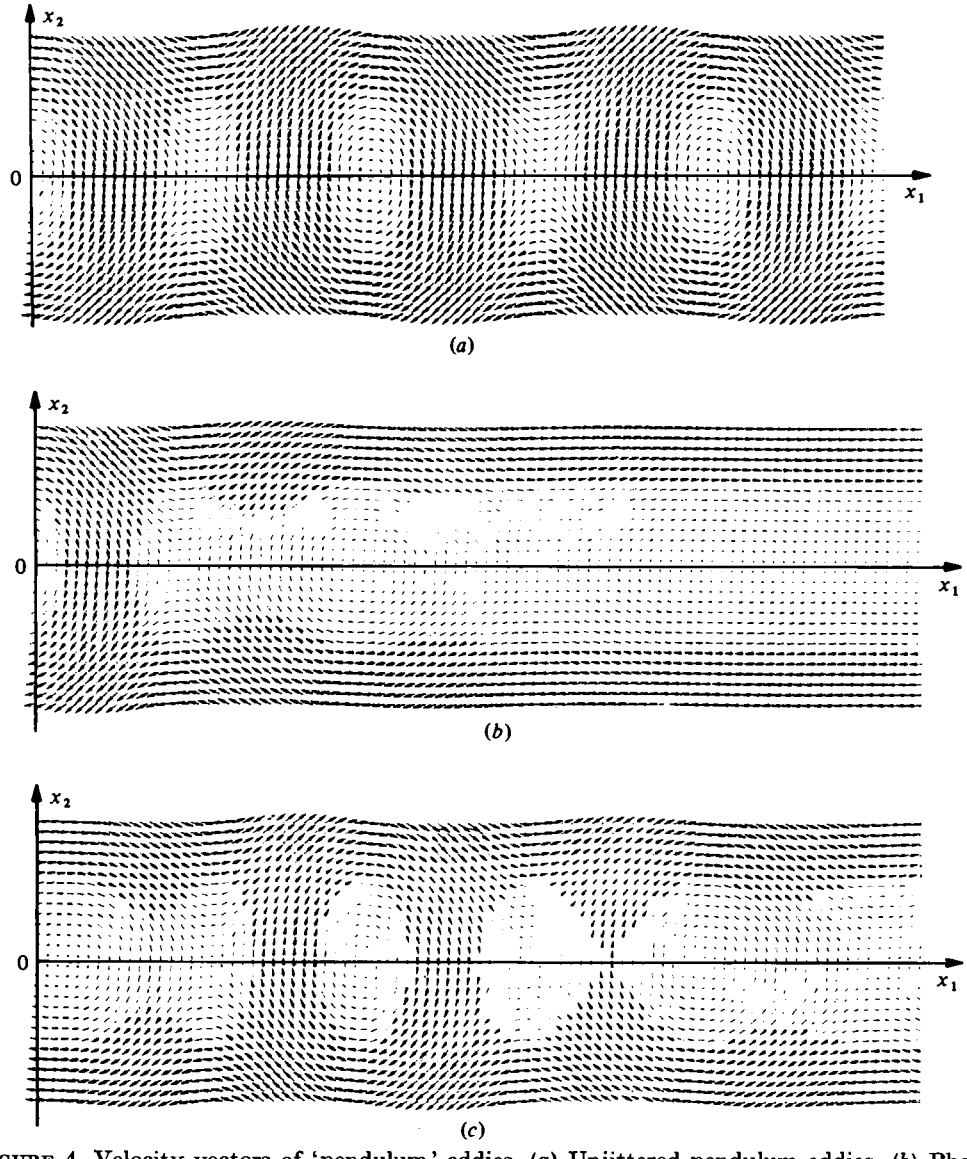

FIGURE 4. Velocity vectors of 'pendulum' eddies. (*a*) Unjittered pendulum eddies. (*b*) Phase-averaged jittered pendulum eddies. (*c*) Same as (*b*) but with the effect of phase shift of filters included.

consider that the entire 'flow field' can be measured simultaneously. Furthermore, restrict the wavelength within each group of 'coherent structures' to be constant but let each group have a different wavelength. By associating a p.d.f. with the wavelength (or frequency) distribution, an artificial 'phase-averaged' representation of the flow field can be produced.

This exercise was performed on a digital computer using an experimentally obtained p.d.f. of the frequency of vortex shedding behind the oblate ellipsoid described in §4. Figure 4(*b*) shows the phase-averaged flow field obtained by jittering the pendulum

eddies with this experimental data. The frequency or wavelength jitter causes washout of the vertical velocity components (no washout occurs for the streamwise velocity components for this particular case, see equation (5)).

For simplicity, a normal distribution can be used to analyse the washout. The vertical velocity component of the pendulum eddies can be expressed as

$$v = -A\sin(px_1). \tag{7}$$

Let p be normally distributed about a mean value $\bar{p}$ with a variance σ. Then

$$\bar{v} = \int_{-\infty}^{\infty} -\frac{A}{\sigma\sqrt{(2\pi)}}\sin px_1 \exp\left\{-\frac{1}{2}\left(\frac{p-\bar{p}}{\sigma}\right)^2\right\} dp \tag{8}$$

and this leads to

$$\bar{v} = -A\left[\exp\{-\tfrac{1}{2}\sigma^2x^2\}\right]\sin(\bar{p}x_1). \tag{9}$$

It can be seen that the averaged vertical velocity component decays with distance downstream.

It was thought that the effect of signal phase shifting by the bandpass filter would cause even greater washout of the data, but the opposite was found to be true. Figure 4(*c*) shows the 'phase-averaged' vector field obtained using the same frequency distribution but with the phase shift of the filters included. The phase shift was calculated by assuming a steady-state sinusoidal filter response and the effect was included by shifting bodily each group of structures relative to the stationary reference.

From these studies it is concluded that the effect of phase jitter is to wash out the downstream regular critical points. Closer to the phase detector the centres and saddles still retain their identity but their strength is diminished. The effect of phase shifting through filters appears to reduce this washout.

Perry *et al.* (1980) have shown that saddles need not necessarily be joined together but that two half saddles may sit on a vortex sheet (the dislocated saddle). Using the notation of figure 5(*a*) the velocity field in the vicinity of this irregular critical point is given by

$$\left.\begin{aligned} u &= a\left(x - \frac{\epsilon_0}{2}e^{-at}\right) \quad \text{for} \quad y > 0, \\ u &= a\left(x + \frac{\epsilon_0}{2}e^{-at}\right) \quad \text{for} \quad y < 0, \\ v &= -ay. \end{aligned}\right\} \tag{10}$$

Again, the isobars belong to a parabola of revolution at O and $a = \sqrt{-P_{xx}}$ where $P_{xx} = P_{yy}$ are the second derivatives of kinematic pressure; ϵ_0 is the value of ϵ at $t = 0$ shown in figure 5(*a*). The strength of the sheet and the dislocation distance ϵ decrease exponentially with time as the sheet is being stretched across the filaments.

The location and development of dislocated saddles will vary from structure to structure due to phase jitter. It is simple to show that dislocated saddles sitting on a zero-thickness vortex sheet appearing at different locations and at different stages of development will produce a phase-averaged critical point at the mean location and at the mean stage of development. It turns out that this phase-averaged structure, in the small and in the large, follows the same equations as found by Perry *et al.* (1980) for a dislocated saddle sitting on a vortex sheet of finite thickness provided the phase-averaged values of vorticity and pressure derivatives are used.

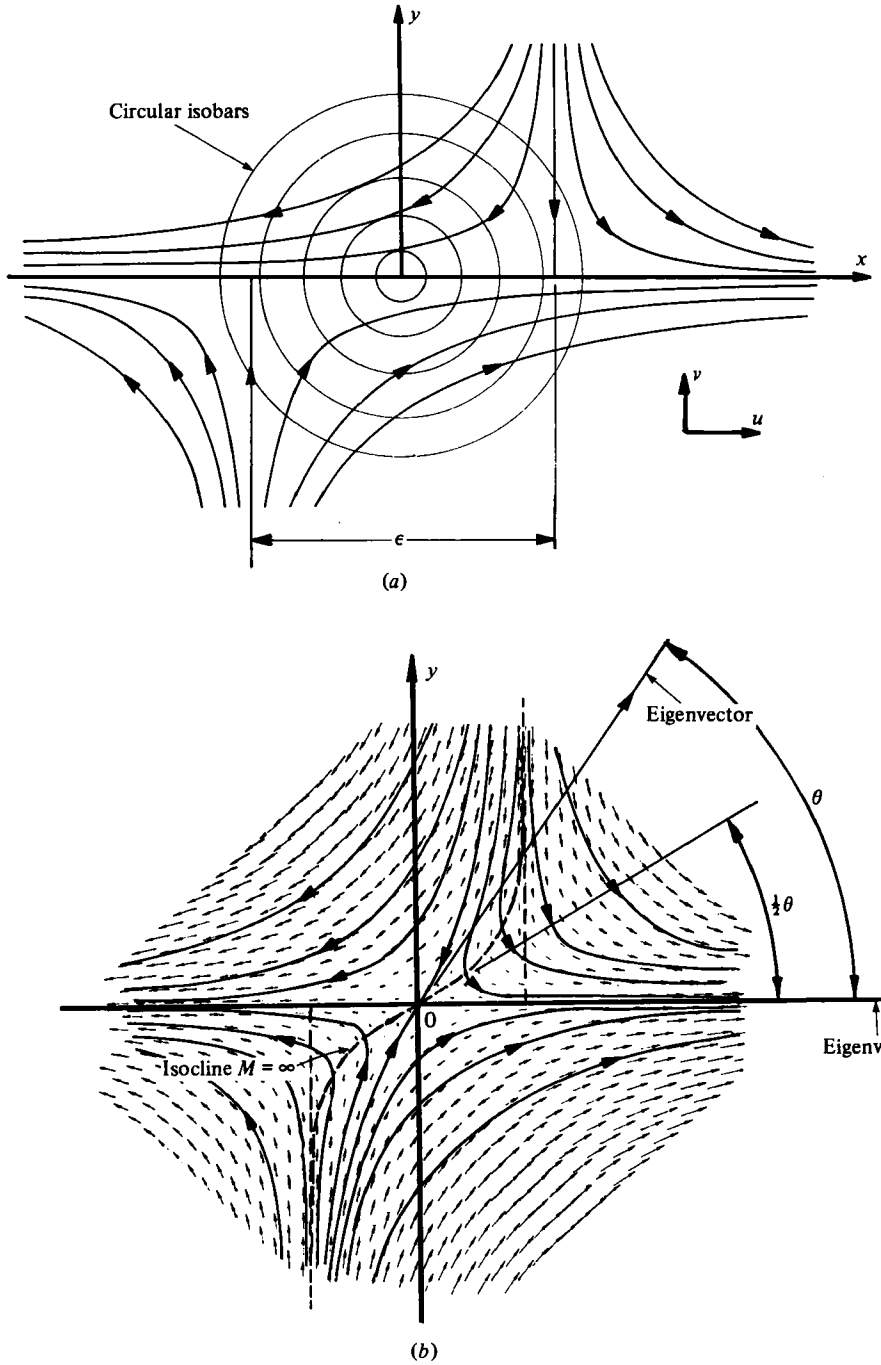

FIGURE 5. (*a*) Instantaneous streamline pattern and notation used for a dislocated saddle sitting on a zero-thickness vortex sheet. (*b*) A phase-averaged dislocated saddle which has been jittered according to a normal distribution. θ given by $\tan\theta = 2a/\eta$ where η is the phase-averaged vorticity (see Perry *et al.* 1980).

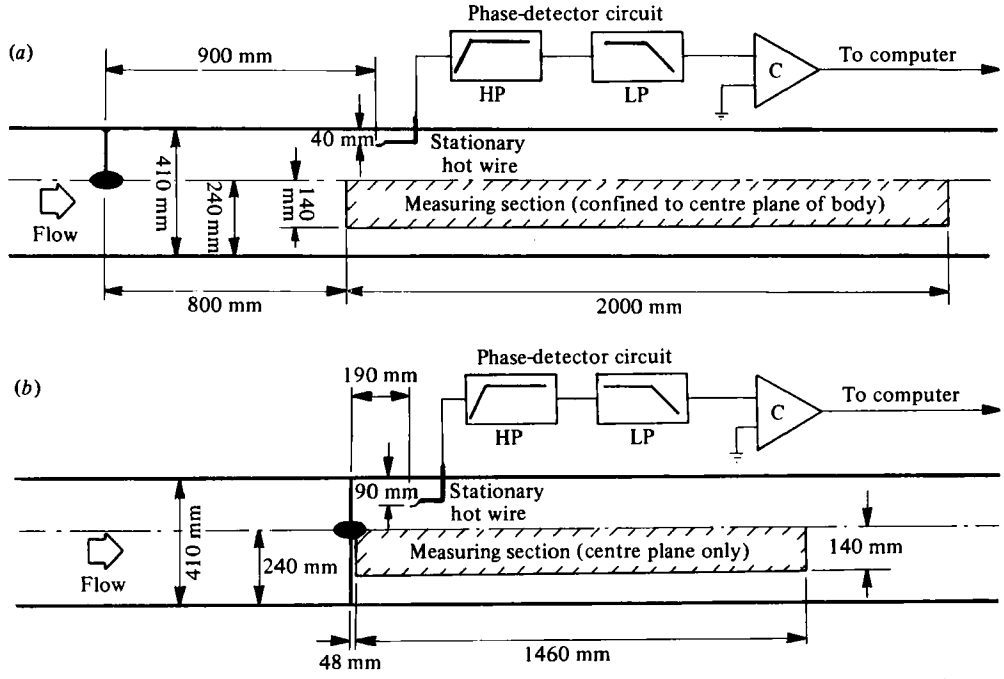

FIGURE 6. Sketch showing position of body relative to measured regions and the stationary phase-detector hot wire. (*a*) Far wake. (*b*) Near wake. LP means low-pass filter. HP means high-pass filter.

Figure 5(*b*) shows the effect of averaging the dislocated saddle given by equation (10) which has been bodily 'jittered' about the mean location according to a normal distribution. The isocline $M = \infty$ and the eigenvectors at the critical point are superimposed on the calculated velocity vector field together with the mean location of the half-saddles and the vortex sheet. In the large, the flow pattern still resembles a dislocated saddle but closer to the critical point the flow resembles a regular saddle in non-canonical form. The vorticity contained in the averaged sheet diminishes as the variance increases. In fact, infinite jitter leads to a regular irrotational saddle.

The phase-averaged patterns produced by jittering all the critical points considered follow Euler's equations of motion if phase-averaged quantities are used. It turns out that the phase-averaged Reynolds stresses have zero gradients at the critical points and so also do the viscous stresses. A further broadening of the region of vorticity will, of course, occur due to the fine-scale Kelvin–Helmholtz-like roll-ups within the sheet. A photograph of such fine-scale roll-ups superimposed on a large-scale roll-up is shown in figure 6 of Pullin & Perry (1980) for a vortex sheet generated at a sharp edge.

4. Results

4.1. *Flow conditions and the detection of coherence*

As was mentioned in the introduction, Perry & Lim (1978) found that the structures in a neutrally buoyant coflowing wake are basically the same (except for the cavity) as those which occur naturally behind a blunt three-dimensional body such as a sphere.

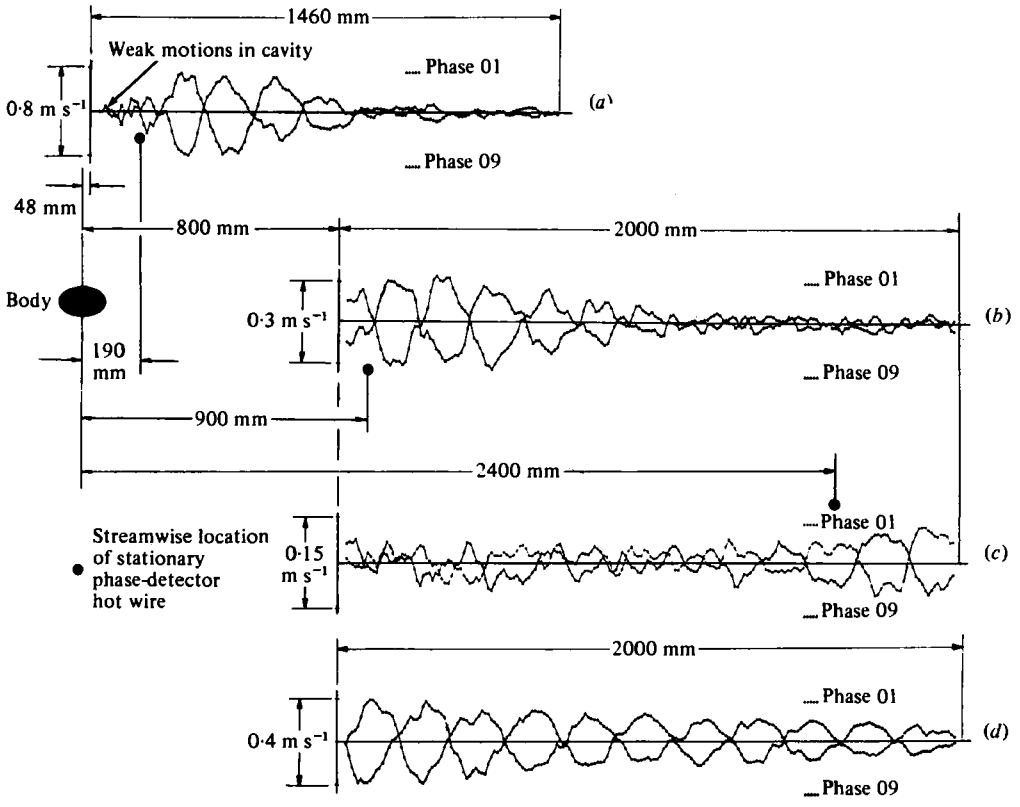

FIGURE 7. The vertical velocity perturbations along the centre-line of body: (*a*) near wake; (*b*) far wake; (*c*) far wake with phase detector shifted downstream; (*d*) far wake of oscillating body.

By distorting the sphere into an oblate ellipsoid the orientation of the structures about a streamwise axis was stabilized. An oblate ellipsoid with a streamwise chord of 127 mm, width of 220 mm and height of 73 mm was built for the purpose of studying the high-Reynolds-number flow case. The shedding of structures behind the body was found to be only very weakly periodic. Two sets of results were obtained. One set was obtained for the near wake and one for the far wake. For the near wake it was necessary to split the body by the mechanism shown in figure 2 to allow the hot-wire probe to pass through. This enabled the wires to possess a high bias velocity in the cavity and allowed valid results to be obtained within 2 cm of the body. The body remained open to allow the wires through and was closed during the return pass of the sled so that a new set of structures was established before the sled began its new sampling cycle. In the far-wake measurements, the body was not split. The free-stream tunnel velocity was 4·29 m s^{-1} and the velocity of the sled was 3·8 m s^{-1}. Figure 6(*a*) and (*b*) show the position of the body, the measured region and the stationary phase-detector hot wire. The phase-detector circuits used in the experiments are also shown. All measurements were confined to the vertical centre-plane of the body and below the streamwise axis.

Fifteen rows of data 10 mm apart were sampled at 10 mm intervals along the measuring sections and 800 sled passes and 5-point smoothing were utilized. The Reynolds number of the wake was 32500 based on the streamwise chord of the body.

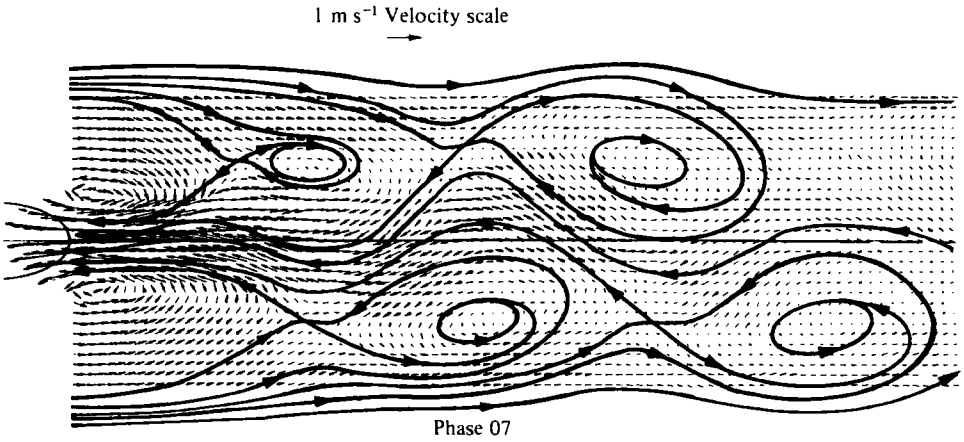

FIGURE 8. One of the sixteen phase-averaged vector fields as seen by an observer moving at the calculated convection velocity (3·9 m s^{-1}) for the near wake. The authors' interpretations of the separatrices (phase-averaged streamlines emanating from saddles) are superimposed.

The positions of the stationary hot wire and the phase detector circuit variables were optimized by trial and error by viewing the animation of the phase-averaged hot-wire voltages mentioned earlier. The phase-averaged vertical velocity perturbations of phases 1 and 9 for the row corresponding to the body centre-line are shown plotted in figure 7(*a*)–(*c*) for each case. The decay of the wave forms bears a resemblance to the decay of the wave forms of the jittered pendulum eddies (see equation (9)). These phases are 180° apart and indicate a form of symmetry about the body centre-line. This type of symmetry and the alternate nature of vortex shedding permit the phase-averaged vector fields to be reflected about the body centre-line thus giving a complete picture of the wake (see Cantwell 1975). Various numerical and graphical methods were applied to determine the average wavelength of the structures. The mean frequency was determined with precision by long time averaging, thus enabling the convection velocity of the eddies to be accurately determined.

A comparison between the near-wake and far-wake results shows that the coherence moves with the phase detector. In fact, figure 7(*c*) shows the far-wake results when the phase detector was moved 2400 mm behind the body. From these results, no large-scale vortex pairing seems to have occurred on average and the structures retain their identity up to 8 structure lengths behind the body.

4.2. *Phase-averaged vector fields*

Sixteen velocity vector fields (representing 48000 velocity vectors) have been plotted for each case studied but not all of these will be presented here owing to the volume of material involved. An animation movie has been made of each case.

Figure 8 shows the phase-averaged vector field of the near wake for phase 7 with the authors' interpretation of phase-averaged streamlines superimposed. The effect of phase jitter and subsequent washout is apparent as predicted by the pendulum eddy simulation, i.e. the strength of the vector field appears to diminish downstream. It can be seen that the separatrices possess the same general geometrical features as

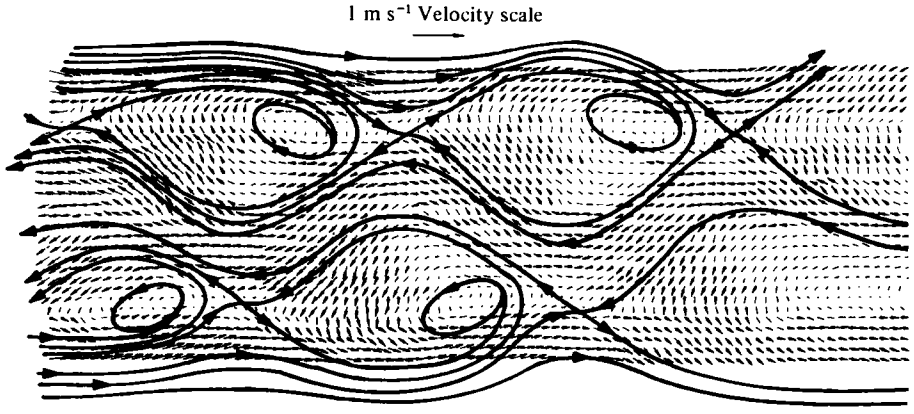

FIGURE 9. One of the sixteen phase-averaged vector fields seen by an observer moving with the structures in the far wake of the ellipsoid with authors' interpretations superimposed. Note the washout in the most downstream eddy giving the appearance of simple horizontal shear.

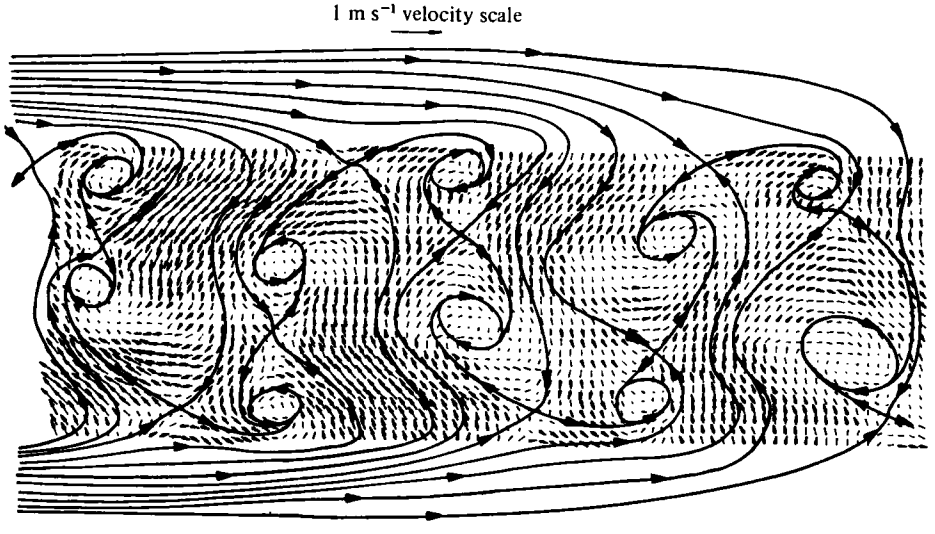

FIGURE 10. One of the sixteen phase-averaged vector fields seen by an observer moving with the structures in the far wake of the oscillating ellipsoid with the authors' interpretations superimposed.

the low-Reynolds-number results of Perry *et al.* for a neutrally buoyant coflowing wake (figure 1). The alleyways discussed by these authors are apparent.

In interpreting these flow patterns the authors were guided by the critical point classification given by Perry *et al.* For instance, in two-dimensional flow only centres and saddles are allowed, whereas in the three-dimensional flow it is permissible to have foci in the large where fluid spirals in, but these spirals must asymptote to centres since the spanwise stretching of these phase-averaged structures is small. Note the clarity of the dislocated saddles in this figure. This is because the vortex sheets are 'fresh and young' and because the first few structures are subject only to a small amount of phase jitter. These dislocated saddles, of course, would differ slightly in

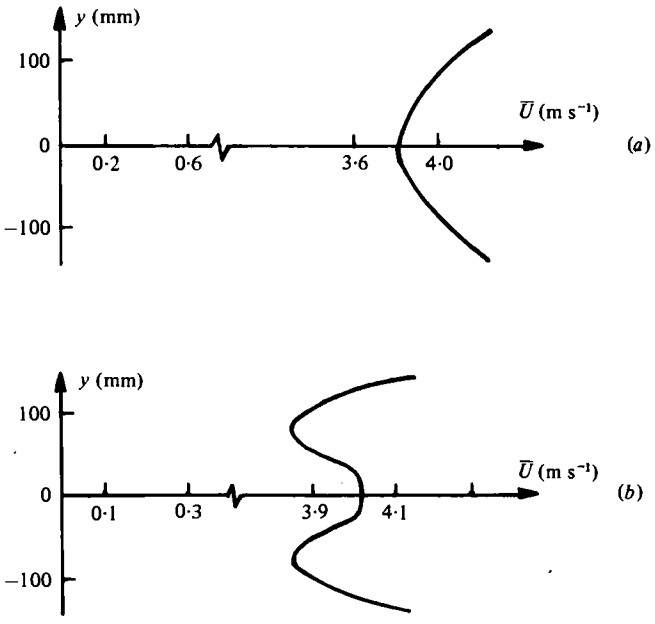

FIGURE 11. Comparison of temporal mean velocity traverses: (*a*) 750 mm downstream of non-oscillating body; (*b*) 800 mm downstream of oscillating body.

detail from those treated in §3. Those in §3 were two-dimensional, i.e. plane stagnation point irrotational saddles. The saddles being observed here would be of a three-dimensional form (see Perry *et al.* 1980).

Figure 9 shows one of the 16 phase-averaged velocity vector fields for the far-wake tests also viewed in a frame of reference moving with the structures. It can be seen that the dislocated saddles are more like regular saddles and appear somewhat merged with the centres to produce a pattern resembling simple horizontal shear. This is the result of substantial phase jitter. When a saddle and a centre of approximately equal strength are combined, this simple shearing pattern is formed.

Overall the general geometrical features of these structures and, in particular, the entrainment pattern of irrotational fluid into these structures are very similar to the low-Reynolds-number results of Perry *et al.*

4.3. *Oscillating body*

As a matter of interest the authors decided to investigate the effect on coherence of oscillating the body at a frequency close to the natural frequency of vortex shedding. Following Perry & Lim (1978) the authors felt that certain simplifications would occur, enabling a more detailed study of these flow patterns. For instance, the phase of vortex shedding could be very accurately determined from the motion of the forcing mechanism and perhaps the phase-averaged results would be greatly enhanced. The body was oscillated $\pm 5°$ about its cross-stream axis at a frequency of 11 Hz. Figure 7(*d*) shows the phase-averaged vertical velocity fluctuations along the row corresponding with the body centreline for phases 1 and 9. The small decay of these structures with streamwise distance is apparent.

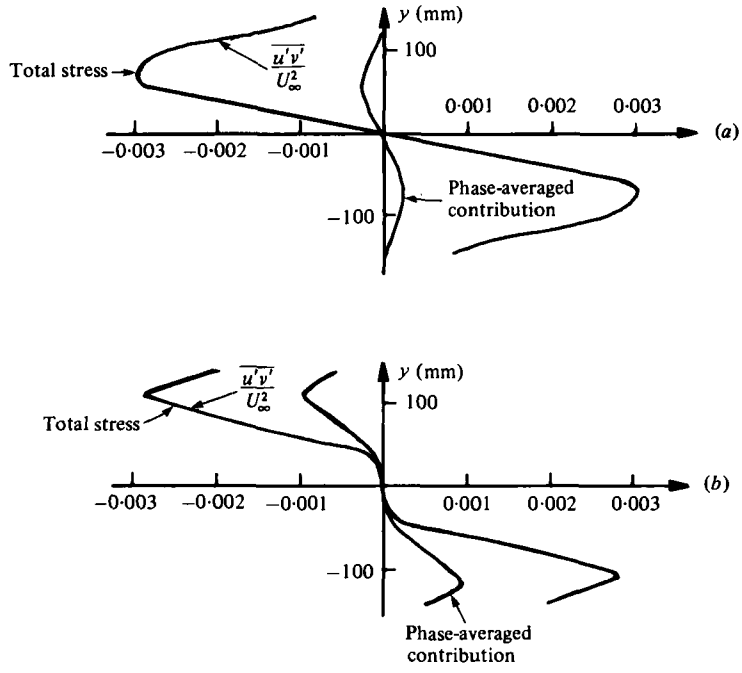

FIGURE 12. Reynolds-stress distribution: (*a*) 750 mm downstream of non-oscillating body; (*b*) 800 mm downstream of oscillating body.

Figure 10 shows one of the 16 phase-averaged vector fields with the authors' interpretation of the separatrices superimposed. A surprising feature of this result is the appearance of centres of opposite vorticity and, from the classification of Perry & Lim, these structures exhibit jet-like qualities. In unpublished work, Perry & Lim observed rather complicated features in their smoke patterns when the amplitude of tube oscillation was too high. Unfortunately, in this experiment the amplitude of rocking of the body was too large to produce a pure wake in the sense of Perry & Lim. Figure 11 shows a comparison of the time-averaged velocity profiles for the two cases. For the oscillating body the flow could be appropriately described as a 'jet-wake'. The jet-like nature of this flow implies that the body is attempting to propel itself through the flow in much the same way as a fish or a bird.

The authors suggest that the apparatus they have constructed and the techniques they have developed could lend themselves to the study of the propulsion of bodies and animals.

4.4. *Reynolds stress*

It is of interest to calculate what contribution the large-scale structures of turbulence contribute to Reynolds stress. Cantwell in his work found that the large-scale phase-averaged structures behind a cylinder contributed up to 50% of the total Reynolds stress. For the results presented here, the authors found the phase-averaged structures contributed only about 15% of the total Reynolds stress. It must be realized that the phase jitter experienced in these experiments was considerably higher than those behind a two-dimensional cylinder, which was verified by cursory tests on a

cylinder during the early stages of this project. The larger amount of phase jitter implies greater washout of the phase-averaged data and, since the Reynolds stress depends on the product of velocity components, the inferred contribution will be considerably reduced.

The most important feature of the Reynolds stress distribution is that the peaks occurred where the centres and saddles were passing. Figure 12(*a*) shows a typical distribution of the total Reynolds stress and the contribution of the phase-averaged structures. The authors believe that the large-scale structures carry more than is implied by these results. This was partially verified in the far wake of the oscillating body. The higher coherence led to a 30% contribution to the total Reynolds stress, as can be seen in figure 12(*b*).

5. Conclusions and discussion

Phase averaging has revealed that coherent large-scale structures exist in wakes behind three-dimensional blunt bodies at high Reynolds numbers. These structures retain their identity for long streamwise distances.

The geometry of the phase-averaged vector field displays the same general features as in the low-Reynolds-number (unsteady laminar flow) wake results of Perry *et al.* (1980). The separatrices emanating from dislocated saddles spiral in towards centres and the irrotational fluid is entrained into the structures in the same way as in the low-Reynolds-number cases. Hence, a vortex loop system revealed in the smoke pictures of Perry & Lim might be appropriate for modelling these large-scale motions.

It would appear that the fine-scale motions are decoupled from the large-scale motions in the following sense. The fine-scale motions act on the larger motions as an 'eddy viscosity'. In the case where no fine-scale motions are present, as in the structures of Perry & Lim, the general features of the eddy geometry were found to be independent of Reynolds number and hence independent of molecular viscosity. By a crude analogy perhaps one could say that, in the turbulent case, the broad features of the large-scale motions are not heavily influenced by the 'eddy viscosity' produced by the fine-scale motions.

The deduced geometrical features of these large-scale motions are independent of the arbitrary choice of the method of phase detection. However, the true strength of these large-scale motions and their contribution to the Reynolds stress and turbulent energy depends on the method of phase detection. Their strength would be greatly enhanced if more sophisticated methods could be devised to account for phase jitter and washout.

The phase-averaged structures were found to contribute between 15 and 30% of the total Reynolds stress. This is thought to be a low estimate due to the large amount of phase jitter experienced in these flows. The results of Cantwell for a cylinder indicate that the contribution may be as high as 50%. The peaks in the Reynolds-stress distribution occur where the centres and saddles are passing.

The power of critical-point theory in describing these structures is evident. The theory is also useful for investigating the effect of phase jitter on washout.

REFERENCES

CANTWELL, B. J. 1975 A flying hot-wire study of the turbulent near wake of a circular cylinder at a Reynolds number of 140000. Ph.D. thesis, California Institute of Technology.

PAPAILIOU, D. D. & LYKOUDIS, P. S. 1974 Turbulent vortex streets and the entrainment mechanism of the turbulent wake. *J. Fluid Mech.* **62**, 11.

PERRY, A. E. & FAIRLIE, B. D. 1974 Critical points in flow patterns. *Advances in Geophysics* B **18**, 299.

PERRY, A. E. & FAIRLIE, B. D. 1975 A study of turbulent boundary-layer separation and re-attachment. *J. Fluid Mech.* **69**, 657–672.

PERRY, A. E. & LIM, T. T. 1978 Coherent structures in coflowing jets and wakes. *J. Fluid Mech.* **88**, 451.

PERRY, A. E., LIM, T. T. & CHONG, M. S. 1980 The instantaneous velocity fields of coherent structures in coflowing jets and wakes. *J. Fluid Mech.* **101**, 243.

PERRY, A. E. & MORRISON, G. L. 1971 Static and dynamic calibrations of constant-temperature hot-wire systems. *J. Fluid Mech.* **47**, 765.

PULLIN, D. I. & PERRY, A. E. 1980 Some flow visualization experiments on the starting vortex. *J. Fluid Mech.* **97**, 239.

WATMUFF, J. H. 1979 Phase-averaged large-scale structures in three-dimensional turbulent wakes. Ph.D. thesis, University of Melbourne.